

Non-Hermiticity induced thermal entanglement phase transition

Bikashkali Midya

Indian Institute of Science Education and Research Berhampur, Odisha 760003, India

Theoretical analysis of a prototypical two-qubit effective non-Hermitian system characterized by asymmetric Heisenberg XY interactions in the absence of external magnetic fields demonstrates that maximal bipartite entanglement and quantum phase transitions can be induced exclusively through non-Hermiticity. At thermal equilibrium as $T \rightarrow 0$, the system attains maximal entanglement $C = 1$ for values of the non-Hermiticity parameter greater than a critical value $\gamma > \gamma_c = J\sqrt{1 - \delta^2}$, where J denotes the exchange interaction and δ represents the anisotropy of the system; conversely, for $\gamma < \gamma_c$, entanglement is nonmaximal and given by $C = \sqrt{1 - (\gamma/J)^2}$. The entanglement undergoes a discontinuous transition to zero precisely at $\gamma = \gamma_c$. This phase transition originates from the closing of the energy gap at a non-Hermiticity-driven ground state degeneracy, which is fundamentally different from an exceptional point. This work suggests the use of singular-value-decomposition generalized density matrix for the computation of entanglement in bi-orthogonal systems.

Introduction.— Certain non-Hermitian open quantum systems exhibit exceptional point (EP) spectral singularities, where multiple eigenfrequencies coalesce and their corresponding eigenstates become indistinguishable^{1,2}. These points were initially investigated in semi-classical systems³, leading to phenomena such as EP-induced lasing, non-reciprocal dynamics, and enhanced sensing capabilities (refer to the reviews⁴⁻⁶ and references therein). Subsequently, EPs have been identified as producing novel quantum effects such as universal critical phenomena⁷⁻⁹, accelerated relaxation process¹⁰, chiral state transfer¹¹, and have been observed in various dissipative quantum systems, including solid-state spins¹²⁻¹⁵, trapped ions¹⁶⁻¹⁸, ultracold gases¹⁹⁻²¹, superconducting and quantum photonic qubits²²⁻²⁵. In contemporary research, non-Hermitian interactions and EPs are emerging as key resources in the field of quantum information science²⁶, and the investigation of entanglement and its dynamics²⁷⁻⁵³. Specifically, investigations have revealed nontrivial quantum advantages such as faster-than-Hermitian entanglement generation²⁸, chiral exchange of Bell states²⁹, and entanglement filtering within non-Hermitian coupled qubit systems²⁷.

These advancements naturally lead to an important question: *Can non-Hermiticity alone induce maximal thermal entanglement⁵⁴⁻⁵⁶ and trigger phase transitions in otherwise Hermitian qubit system that do not exhibit these features in the absence of external magnetic fields?* Here, we provide an affirmative answer to this important question. By examining a minimal model of two asymmetrically coupled spin qubits, it is demonstrated that maximal entanglement can be attained by tuning the effective non-Hermitian parameter beyond the point where the spectral energy gap closes. Notably, this gap-closing point is shown to differ from an EP, as the corresponding states remain distinguishable. This finding contrasts with prior investigations on analogous Hermitian models^{54,55,57,58}, which suggested that external magnetic fields are requisite for attaining

thermal entanglement transition. Furthermore, this work introduces singular-value-decomposition (SVD) generalized thermal states, which accurately captures the entanglement characteristics of non-Hermitian systems.

Theoretical model.— We consider an effective non-Hermitian systems defined by the Hamiltonian $H = H_{XY} + H_{NH}$, where the Heisenberg XY Hamiltonian for two qubit systems having nearest-neighbor interaction is given by⁵⁶

$$H_{XY} = 2J \left[(1 + \delta) S_1^x S_2^x + (1 - \delta) S_1^y S_2^y \right]. \quad (1)$$

Here, the operators $S_n^{x,y,z} = \sigma_n^{x,y,z}/2$, defined in terms of the Pauli matrices, correspond to the local spin- $\frac{1}{2}$ operator at qubit n , $J > 0$ is the antiferromagnetic exchange interaction, and the dimensionless parameter δ ($0 \leq \delta \leq 1$) denotes anisotropy of the system; specifically, $\delta = 0$ characterizes an isotropic interaction, whereas $\delta = 1$ corresponds to a fully anisotropic Heisenberg-Ising interaction. When δ equals 1, the Hamiltonian H_{XY} does not exhibit thermal entanglement⁵⁵. Additionally, a quantum phase transition is not observed for values of $\delta < 1$ unless an external tunable parameter, such as an applied magnetic field, is introduced^{54,55,57,58}. The non-Hermitian component of the Hamiltonian is given by

$$H_{NH} = \gamma_1 S_1^- S_2^+ + \gamma_2 S_1^+ S_2^-, \quad (2)$$

where $S_n^\pm = S_n^x \pm iS_n^y$ are creation and annihilation operators, and $\gamma_1 \neq \gamma_2^*$ parameterize the rate of asymmetric exchange between two qubits in the subspace $\{|\uparrow\downarrow\rangle, |\downarrow\uparrow\rangle\}$ spanned by single spin excitations. For analytical tractability, we impose an anti-Hermitian condition $H_{NH}^\dagger = -H_{NH}$ satisfied by $\gamma_1 = -\gamma_2 = \gamma$. Under this assumption, the total Hamiltonian simplifies to

$$H = (J + \gamma) S_1^- S_2^+ + (J - \gamma) S_1^+ S_2^- + J\delta(S_1^- S_2^- + S_1^+ S_2^+). \quad (3)$$

The Hamiltonian (3), apart from an overall dissipative term ($-i\gamma$), represents the effective Hamiltonian of a fully postselected Markovian open quantum system⁵⁹⁻⁶¹. This

Hamiltonian can be derived from the Lindblad master equation (with $\hbar = 1$)⁶² given by:

$$\frac{d\rho(t)}{dt} = \mathcal{L}\rho(t) = -i[H_{XY}, \rho] + \mathcal{D}[L_{12}]\rho + \mathcal{D}[G_{12}]\rho, \quad (4)$$

Here, ρ is the density operator of the system, and \mathcal{L} denotes a hybrid Liouvillian that includes the coupled spin Hamiltonian H_{XY} , which governs the coherent evolution of the system. The operators L_{12} and G_{12} are pairwise jump operators^{63–65} defined as:

$$L_{12} = \sqrt{\frac{\gamma}{2}}(S_1^- - iS_2^-), \quad G_{12} = \sqrt{\frac{\gamma}{2}}(S_1^+ + iS_2^+), \quad (5)$$

These operators characterize the system's nonunitary interaction with its environment through a generalized dissipator⁶¹:

$$\mathcal{D}[Z]\rho = 2qZ\rho Z^\dagger - (Z^\dagger Z\rho + \rho Z^\dagger Z). \quad (6)$$

Here, $\gamma > 0$ represents the rate of dissipative interaction, while the parameter $q \in [0, 1]$ controls the degree of postselection dynamics: $q = 0$ corresponds to full postselection dynamics, whereas $q = 1$ indicates no postselection. The Liouvillian in equation (4) can be expressed as

$$\mathcal{L}\rho = -i(H_{\text{eff}}\rho - \rho H_{\text{eff}}^\dagger) + q(2L_{12}\rho L_{12}^\dagger + 2G_{12}\rho G_{12}^\dagger), \quad (7)$$

where the effective non-Hermitian Hamiltonian reduces to

$$H_{\text{eff}} = H_{XY} - iL_{12}^\dagger L_{12} - iG_{12}^\dagger G_{12} = H - i\gamma. \quad (8)$$

This final equality is derived using the relations $\{S_1^-, S_1^+\} = \{S_2^-, S_2^+\} = 1$ and $[S_1^-, S_2^+] = 0$. When postselected trajectories of null quantum jump is chosen (i.e., $q = 0$), equations (7) and (4) show that the Lindblad master equation simplifies to the von Neumann equation. In this scenario, the dynamical solution given by $\rho(t) = e^{-itH_{\text{eff}}}\rho(0)e^{itH_{\text{eff}}^\dagger}$ is formally equivalent to a thermal state $\rho(T)$ through the Wick rotation $it = \frac{1}{k_B T}$. It may be noted that the uniform background loss term ($-i\gamma$) in equation (8) does not affect the thermal entanglement discussed later; therefore, it has been omitted, leading to the approximation $H \simeq H_{\text{eff}}$.

It may be noted that postselected non-Hermitian quantum systems have been experimentally realized in superconducting qubits^{22,23}. The effective Hamiltonian described in Eq. (3) is also significant in cascaded qubit networks, such as when qubits are coupled to a chiral bath^{63,66,67}.

Energy spectrum and degeneracy.— The right- and left-eigenstates of the Hamiltonian H are expressed in the standard two qubit basis $\{|\uparrow\uparrow\rangle, |\uparrow\downarrow\rangle, |\downarrow\uparrow\rangle, |\downarrow\downarrow\rangle\}$:

$$\begin{aligned} |R_{0,3}\rangle &: \frac{1}{\sqrt{2}} \left(\sqrt{\frac{J-\gamma}{J+\gamma}} |\uparrow\downarrow\rangle \mp |\downarrow\uparrow\rangle \right), |R_{1,2}\rangle : \frac{1}{\sqrt{2}} (|\uparrow\uparrow\rangle \mp |\downarrow\downarrow\rangle) \\ |L_{0,3}\rangle &: \frac{1}{\sqrt{2}} \left(\sqrt{\frac{J+\gamma}{J-\gamma}} |\uparrow\uparrow\rangle \mp |\downarrow\downarrow\rangle \right), |L_{1,2}\rangle = |R_{1,2}\rangle, \end{aligned} \quad (9)$$

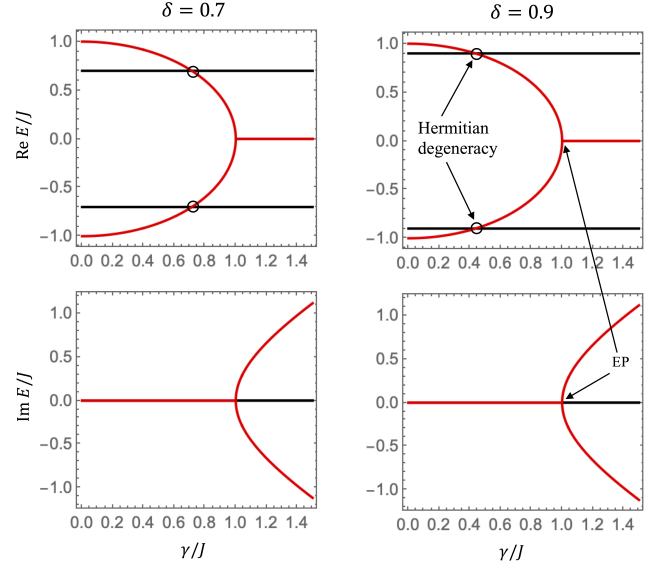


FIG. 1. *Non-Hermiticity induced Hermitian degeneracy.* Energy spectra of H for two distinct values of δ , illustrate the appearance of a Hermitian degeneracy induced by non-Hermiticity, which differs from an exceptional point (EP). When the parameter γ is varied, the ground state and the first excited state interchange their positions. It is also observed that ground-state-interchange takes place at smaller values of γ when δ is larger. This state switching plays a crucial role in the thermal entanglement transition described in the main text. Here, $J = 1$ is chosen.

which satisfy bi-orthonormality condition⁶⁸ $\langle L_j | R_{j'} \rangle = \delta_{jj'}$, and fulfill completeness relation $\sum_j |R_j\rangle \langle L_j| = I$ away from an exceptional point ($\gamma = J$). These eigenstates correspond to a purely real energy spectrum across all values of δ :

$$E_{0,1,2,3} = \{-\sqrt{J^2 - \gamma^2}, -J\delta, J\delta, \sqrt{J^2 - \gamma^2}\}, \quad (10)$$

provided the non-Hermitian parameter satisfies the inequality $\gamma < J$. It may be noted that the non-Hermiticity affects only the states $|R_0\rangle$ and $|R_3\rangle$ corresponding to the energy levels E_0 and E_3 , respectively. As the parameter γ increases, these two energy levels move closer together (see Fig. 1). At $\gamma = J$, the system reaches an exceptional point (EP) where both energies E_0 and E_3 and their associated eigenstates $|R_0\rangle$ and $|R_3\rangle$ merge. For values of $\gamma > J$, a pair of complex conjugate energy levels emerges. In addition to this known EP degeneracy, a novel degeneracy occurs within the intermediate range $0 \leq \gamma < J$, where all energies remain real. This new degeneracy is characterized by two distinct real energy levels becoming equal while their corresponding eigenstates stay distinct and orthogonal. Specifically, the energy gaps between the pairs (E_0, E_1) and (E_2, E_3) simultaneously close when the condition $\gamma/J = \sqrt{1 - \delta^2}$ holds. Figure (1) presents the full energy spectrum of H for different anisotropy parameters

δ , demonstrating how this Hermitian degeneracy arises as the non-Hermiticity parameter γ is varied. This phenomenon, termed ‘non-Hermiticity assisted Hermitian degeneracy’ and distinct from an EP, plays a crucial role in controlling low-temperature thermal entanglement and phase transitions, as explained below. In this paper, we do not discuss entanglement in the situation of complex spectrum $E_j^R = (E_j^L)^*$ for $\gamma > J$, in order to preclude non-unitary dynamical evolution.

Non-Hermiticity induced thermal entanglement and phase transition.— To examine the thermal entanglement in the system, we employ the bi-orthogonal density operator in thermal equilibrium defined as^{54,68} $\rho(T) = Z^{-1} e^{-H/k_B T}$, where

$$e^{-H/k_B T} = \sum_{j=0}^3 e^{-E_j/k_B T} |R_j\rangle\langle L_j|, \quad (11)$$

and $Z = \text{Tr} e^{-H/k_B T}$ denotes the partition function. We have used the above mentioned biorthogonal completeness relation and the trace is defined as $\text{Tr}(\cdot) = \sum_j \langle L_j | \cdot | R_j \rangle$. Here, T is the temperature and k_B is the Boltzmann constant (which is set to unity). The density matrix explicitly given by

$$\rho = \frac{1}{Z} \begin{bmatrix} \cosh \frac{J\delta}{T} & 0 & 0 & -\sinh \frac{J\delta}{T} \\ 0 & \cosh \frac{\sqrt{J^2-\gamma^2}}{T} & -\sqrt{\frac{J-\gamma}{J+\gamma}} \sinh \frac{\sqrt{J^2-\gamma^2}}{T} & 0 \\ 0 & -\sqrt{\frac{J+\gamma}{J-\gamma}} \sinh \frac{\sqrt{J^2-\gamma^2}}{T} & \cosh \frac{\sqrt{J^2-\gamma^2}}{T} & 0 \\ -\sinh \frac{J\delta}{T} & 0 & 0 & \cosh \frac{J\delta}{T} \end{bmatrix} \quad (12)$$

where $Z = 2(\cosh \frac{\delta J}{T} + \cosh \frac{\sqrt{J^2-\gamma^2}}{T})$, is non-Hermitian $\rho^\dagger \neq \rho$. To ensure consistent computation of entanglement measure (see the detailed discussion in Appendix A and the accompanying figure (5)), here we introduce the SVD generalized density matrix⁷¹

$$\rho^{SVD}(T) = \frac{\sqrt{\rho^\dagger(T)\rho(T)}}{\text{Tr} \sqrt{\rho^\dagger(T)\rho(T)}} = \frac{\sqrt{e^{-H^\dagger/k_B T} e^{-H/k_B T}}}{\text{Tr} \sqrt{e^{-H^\dagger/k_B T} e^{-H/k_B T}}}. \quad (13)$$

Note that $\rho^{SVD} = \rho$ when H is Hermitian. The degree of entanglement between two qubits is quantified by the concurrence⁷² defined by $C = \max\{\lambda_0 - \lambda_1 - \lambda_2 - \lambda_3, 0\}$, where λ_j are non-negative eigenvalues, arranged in decreasing order, of the operator

$$R = \left[\rho^{SVD}(\sigma^y \otimes \sigma^y) \rho^{SVD*}(\sigma^y \otimes \sigma^y) \right]^{\frac{1}{2}}. \quad (14)$$

The concurrence ranges from 0 to 1, with a value of zero indicating the absence of entanglement and a value of one corresponding to maximal entanglement between two qubits. As shown in Appendix-A, for (non-degenerate) pure states $\rho_j = |R_j\rangle\langle L_j|$, the concurrence

$$C(\rho_j) = \sqrt{1 - (\gamma/J)^2}, \quad j = 0, 3, \quad (15)$$

and $C(\rho_j) = 1$ for $j = 1, 2$. This indicates that, while the energy eigenstates $|R_1\rangle$ and $|R_2\rangle$ are maximally entangled Bell states, the states $|R_0\rangle$ and $|R_3\rangle$ exhibit non-maximal entanglement in the presence of non-Hermiticity; in fact, they become separable at the exceptional point $\gamma = J$.

The entanglement characteristics in the thermally mixed state described by equation (12) exhibit richer complexity. In general, the concurrence valid for all temperature and system parameters can not be studied analytically. Numerically computed results obtained from Eq. (12) are exemplified in Fig. 2 and Fig. 3. To gain analytical insight into the system’s low temperature entanglement, here we approximate the mixed state by considering only lowest populated ground and first excited states with Boltzmann weight $e^{-E_0/T}/(e^{-E_0/T} + e^{-E_1/T})$ and $e^{-E_1/T}/(e^{-E_0/T} + e^{-E_1/T})$, respectively. This approximation is valid within the temperature range $0 \leq T \leq |E_1 - E_0|$ and away from exceptional point (i.e. at $\gamma = J$, where 2nd excited state also become relevant). In this case, eigenvalues $\lambda_{0,1,2,3}$ of R are given by (detail calculations are provided in Appendix-B)

$$\{\lambda e^{J\delta/T}, \lambda e^{\sqrt{J^2-\gamma^2}/T}, 0, 0\}, \quad (16)$$

when $J\delta > \sqrt{J^2-\gamma^2}$, whereas, first two eigenvalues switch their positions if $J\delta < \sqrt{J^2-\gamma^2}$. Here, $\lambda = \sqrt{J^2-\gamma^2}/(J e^{\sqrt{J^2-\gamma^2}/T} + \sqrt{J^2-\gamma^2} e^{J\delta/T})$. The concurrence $C = \max\{\lambda_0 - \lambda_1, 0\}$ reduces to

$$C(T) = \frac{\sqrt{J^2-\gamma^2}}{J e^{\frac{\sqrt{J^2-\gamma^2}}{T}} + \sqrt{J^2-\gamma^2} e^{\frac{J\delta}{T}}} |e^{\frac{\sqrt{J^2-\gamma^2}}{T}} - e^{\frac{J\delta}{T}}| \quad (17)$$

$$\stackrel{T \rightarrow 0}{=} \begin{cases} \sqrt{J^2-\gamma^2}/J, & \gamma < J\sqrt{1-\delta^2} \\ 0, & \gamma = J\sqrt{1-\delta^2} \\ 1, & \gamma > J\sqrt{1-\delta^2} \end{cases}$$

Equation (17) represents a key finding, and is valid for all values of δ , $0 \leq \gamma < J$ and $T \sim 0$. Following important conclusions are drawn from this equation.

i. First, we discuss entanglement of thermal states in the Heisenberg-Ising system ($\delta = 1$). Interestingly, the concurrence C reaches 1 at absolute zero temperature ($T = 0$) whenever $\gamma \gtrsim 0$. The emergence of maximal entanglement at zero temperature in the non-Hermitian Ising model can intuitively be explained by analyzing the ground state characteristics. For $\gamma = 0$, corresponding to a Hermitian system, the thermal state is separable and consists of an equal mixture of degenerate ground and first excited eigenstates, both of which are maximally entangled^{55,57}. The introduction of non-Hermiticity lifts this degeneracy in a manner distinct from the effect caused by an external magnetic field in Hermitian systems, as illustrated in Figures 2d and 2e. Specifically, increasing γ causes

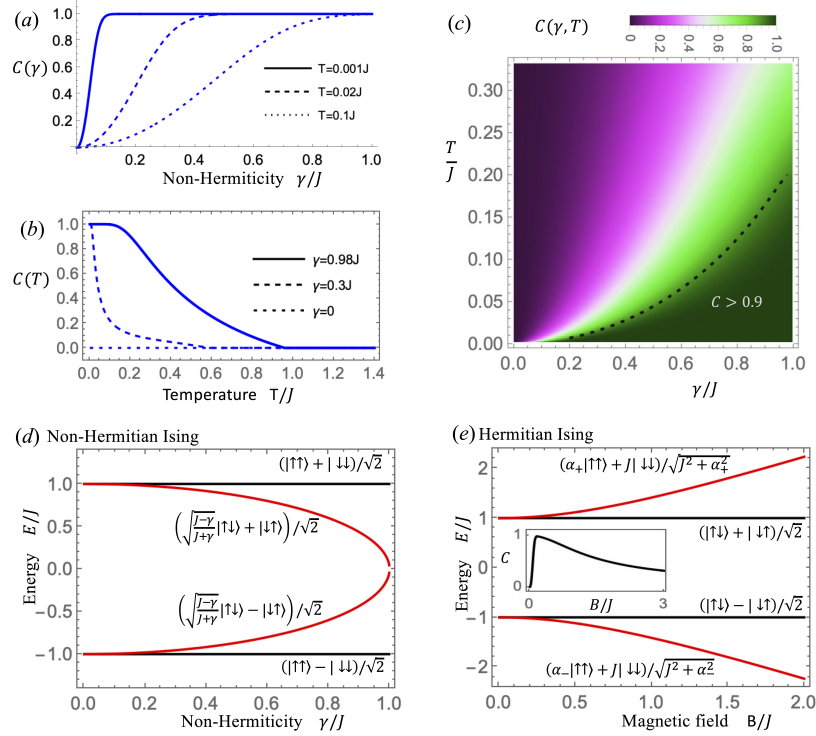


FIG. 2. *Thermal entanglement in the non-Hermitian Heisenberg-Ising model* ($\delta = 1$). (a) The concurrence C , calculated from the thermal mixed state ρ as defined in Eq. (12), is presented as a function of γ at three distinct temperatures. At temperature near zero, entanglement reaches its maximum for non-zero values of γ , whereas at finite temperatures, a stronger non-Hermiticity is required to achieve comparable entanglement. In panel (b), the concurrence C is plotted against temperature for three different values of γ , illustrating an exponential decay of entanglement with increasing temperature. Panel (c) depicts C within the entire parameter range $0 \leq T \leq J/3$ and $0 \leq \gamma < J$. Region below the dashed line represents concurrence $C > 0.9$, follows from the Eq. (18). Maximal entanglement observed at $T = 0$ originates from the non-Hermiticity-assisted non-degenerate ground state, which corresponds to a Bell state, as shown in panel (d). This behavior contrasts sharply with that of the Hermitian system subjected to an external transverse field $B\hat{z}$, described by $H = H_{XY} + B(S_1^z + S_2^z)$; its ground state is non-maximally entangled. Corresponding energy spectrum, $\{\pm\sqrt{J^2 + B^2}, \pm J\}$, and zero temperature concurrence are provided in panel (e) for comparison, where $\alpha_{\pm} = B \pm \sqrt{J^2 + B^2}$.

the first and second excited states within the single spin excitation subspace $\{|\uparrow\downarrow\rangle, |\downarrow\uparrow\rangle\}$ to approach an exceptional point. This transition elevates the maximally entangled triplet Bell state $(|\uparrow\uparrow\rangle - |\downarrow\downarrow\rangle)/\sqrt{2}$ to become the ground state of the system. This effect is termed non-Hermiticity-induced maximal thermal entanglement and represents a mechanism fundamentally different from magnetically induced entanglement found in Hermitian Ising models (see, for example, 57).

ii. For $\delta = 1$ and a specified γ , the first equation of Eq. (17) indicates that the system generates concurrence $> C$, for all temperatures bounded by

$$T < (J^2 - \sqrt{J^2 - \gamma^2}) / \ln \frac{CJ + \sqrt{J^2 - \gamma^2}}{(1 - C)\sqrt{J^2 - \gamma^2}}. \quad (18)$$

The above inequality provides the low temperature estimation of γ and T for a desirable C . Numerical results shown in Figs. 2a and 2c demonstrate that achieving comparable entanglement at finite temperatures requires

stronger non-Hermiticity.

iii. In systems exhibiting anisotropy with $0 < \delta < 1$, the presence of non-Hermiticity leads to a quantum phase transition marked by an abrupt behaviour change from non-maximal to maximal entanglement at zero temperature ($T = 0$). This transition takes place exactly at the critical point $\gamma_c/J = \sqrt{1 - \delta^2}$, as shown in Figures 3a and 3c. The underlying mechanism can be understood by examining the ground state characteristics: for values of γ below γ_c , the ground state is a non-maximally entangled singlet state $|R_0\rangle$. When γ surpasses γ_c , the ground state shifts to $|R_1\rangle$, which is a maximally entangled triplet Bell state. At the critical threshold $\gamma = \gamma_c$, where entanglement drops to zero, this coincides with the spectral degeneracy condition $E_0 = E_1$ (refer to Figures 3c and 3d). Furthermore, an increase in the anisotropy parameter δ corresponds to a decrease in the critical value of γ_c at which this phase transition occurs. Numerical results presented in figure 3b

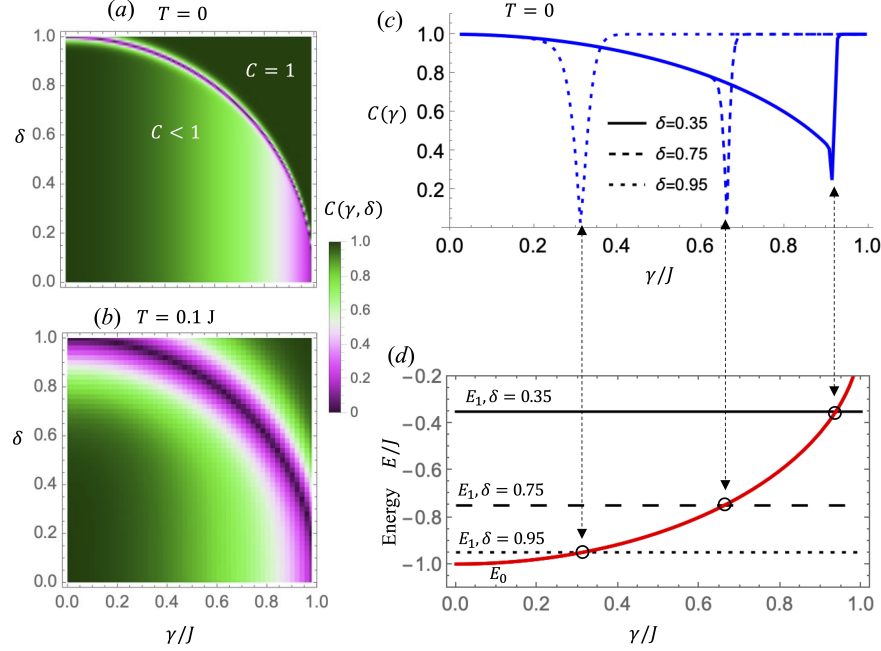


FIG. 3. *Non-Hermiticity induced thermal entanglement phase transition.* Thermal concurrence at absolute zero temperature ($T = 0$) and at $T = 0.1J$ is shown in panels (a) and (b), respectively, across the full range of the anisotropy parameter $0 \leq \delta \leq 1$ and non-Hermiticity $0 \leq \gamma < J$. The results indicate that entanglement experiences a discontinuous transition from $C = 1$ when $\gamma > \gamma_c$ to $C = 0$ exactly at the critical point $\gamma_c = J(1 - \delta^2)^{1/2}$, followed by an asymptotic increase for values of $\gamma < \gamma_c$. This sharp discontinuity in zero temperature entanglement at the critical non-Hermiticity γ_c serves as a hallmark of quantum phase transition. Panel (c) shows that the discontinuity shifts toward lower values of γ as δ increases. Panel (d) shows that the entanglement phase transition coincides with the occurrence of non-Hermiticity-assisted Hermitian degeneracy where $E_0 = E_1$ (marked by circles), where a change in the ground state from a non-maximally entangled to a maximally entangled state as a function of γ occurs.

also indicate that this behavior of entanglement phase transition remains observable at finite temperatures.

iv. In the case of isotropic Heisenberg interaction ($\delta = 0$), the entanglement decreases as γ increases. When γ reaches the value J , all four energy levels become degenerate, resulting in the system being maximally mixed with the density matrix given by $\rho = \mathbb{I}/4$ (see Eq. (12)).

In general, for arbitrary values of γ_1 and γ_2 , the ground state of H is the Bell state $|R_1\rangle$ when the condition $E_1 < E_0$ holds, where $E_0 = -\sqrt{(J + \gamma_1)(J + \gamma_2)}$ and $E_1 = -J\delta$. If this condition is not met, the ground state corresponds to a nonmaximally entangled state characterized by its concurrence

$$C = \frac{2\sqrt{(J + \gamma_1)(J + \gamma_2)}}{2J + \gamma_1 + \gamma_2}. \quad (19)$$

Therefore, the entanglement behavior at zero temperature changes along the energy-gap-closing contours defined by $E_0 = E_1$. A phase diagram illustrating this behavior of entanglement transition for various values of the parameters $(\gamma_1, \gamma_2, \delta)$ is presented in figure (4), whereas complete eigensolutions of H are discussed in Appendix C.

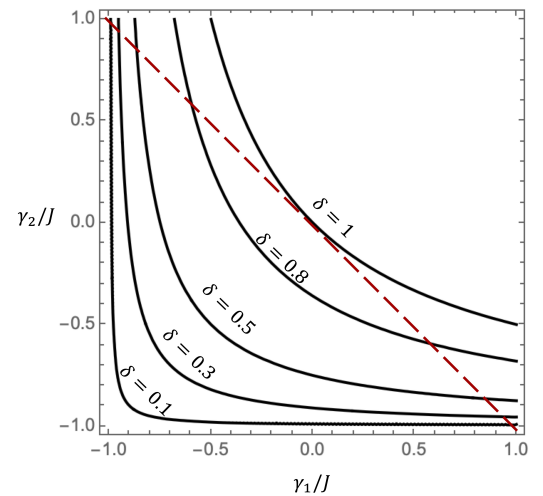


FIG. 4. The contour lines defined by the equation $(J + \gamma_1)(J + \gamma_2) = J^2\delta^2$ in the (γ_1, γ_2) parameter plane indicate the transition in ground-state entanglement from maximal to nonmaximal values for different anisotropy δ . For each specific δ , the entanglement remains maximal below the corresponding contour line, while above it, the entanglement becomes nonmaximal. The special case of $\gamma_1 = -\gamma_2$ is shown by the dashed line.

The ground-state entanglement transition can also be induced by considering the following effective non-Hermitian Hamiltonian

$$\bar{H} = H_{XY} - i\gamma S_1^+ S_1^- - i\gamma S_2^- S_2^+, \quad (20)$$

which correspond to an open system with Lindblad jump operators $L_1 = \sqrt{\gamma} S_1^-$ and $L_2 = \sqrt{\gamma} S_2^+$ acting locally on qubit 1 and qubit 2, respectively. The real part of the spectrum of \bar{H} can be easily confirmed to be isospectral with that of H in Eq. (10): $\text{Spec}(\bar{H}) = \text{Spec}(H) - i\gamma$. And the entanglement properties of both H and \bar{H} are also comparable. Specifically, the ground state spectral and entanglement transition occurs at $\gamma/J = \sqrt{1 - \delta^2}$. Beyond this transition point, the ground state becomes independent of the non-Hermitian parameter γ and corresponds to the Bell state $|R_1\rangle$. Thermal entanglement in models similar to Eq. (20) has been examined in the presence of external fields in references^{69,70}.

Conclusion.— Although the experimental realization of effective non-Hermitian spin models, such as that described by Eq. (3), remains uncertain, theoretical analysis reveals that non-Hermitian interactions alone are capable of inducing maximal bipartite thermal entanglement and its associated phase transition in the absence of external magnetic fields. The method of postselected trajectories of no quantum jumps is considered essential for observing these phenomena in the steady-state dynamics. This necessity arises because the ground states of effective Hamiltonians studied here do not correspond to the dark states of the associated Liouvillian. As a result, stochastic interactions with the environment significantly alter the entanglement characteristics of the system compared to those predicted by an effective Hamiltonian. Extending this theoretical framework to postselected systems comprising a larger number of spins and exploring many-body entanglement^{56,73} merit further research.

Appendix A: Why ρ^{SVD} ?

Here we elaborate with a simple example why ρ^{SVD} is suitable in the computation of entanglement in bi-orthogonal systems. Consider a bi-orthogonal eigenstate, such as $|R_0\rangle = \frac{1}{\sqrt{2}} \left(\sqrt{\frac{J-\gamma}{J+\gamma}} |\uparrow\downarrow\rangle - |\downarrow\uparrow\rangle \right)$. It is evident that this state becomes separable at the EP $\gamma = J$; otherwise, it remains non-separable and thus entangled. Additionally, the degree of entanglement is expected to decrease as γ increases. To quantify the entanglement, we first consider two-qubit bi-orthogonal density matrix

$$\begin{aligned} \rho &= |R_0\rangle\langle L_0| \\ &= \frac{1}{2} \left(|\uparrow\downarrow\rangle\langle\uparrow\downarrow| - \sqrt{\frac{J-\gamma}{J+\gamma}} |\uparrow\downarrow\rangle\langle\downarrow\uparrow| - \sqrt{\frac{J+\gamma}{J-\gamma}} |\downarrow\uparrow\rangle\langle\uparrow\downarrow| + |\downarrow\uparrow\rangle\langle\downarrow\uparrow| \right), \end{aligned} \quad (A1)$$

in matrix form

$$\rho = \frac{1}{2} \begin{pmatrix} 0 & 0 & 0 & 0 \\ 0 & 1 & -\sqrt{\frac{J-\gamma}{J+\gamma}} & 0 \\ 0 & -\sqrt{\frac{J+\gamma}{J-\gamma}} & 1 & 0 \\ 0 & 0 & 0 & 0 \end{pmatrix}, \quad (A2)$$

which is non-Hermitian $\rho^\dagger \neq \rho$. The reduced density matrix $\rho^1 = \text{Tr}_2(\rho) = \frac{1}{2} (|\uparrow\rangle\langle\uparrow| + |\downarrow\rangle\langle\downarrow|)$, for the first qubit, corresponds to the von-Neumann entropy $S = -x_1 \log_2 x_1 - x_2 \log_2 x_2 = 1$, where $x_1 = x_2 = \frac{1}{2}$ are the eigenvalues of ρ^1 . This shows that the system is maximally entangled irrespective of the strength of non-Hermiticity defined by γ . This is a contradiction with our intuitive separability requirement for the state at $\gamma \rightarrow J$.

Other measure of entanglement⁷² e.g. the concurrence $C = \frac{1}{\sqrt{1 - (\gamma/J)^2}}$ obtained from eigenvalues $\{\frac{J}{\sqrt{J^2 - \gamma^2}}, 0, 0, 0\}$ of $R = [\rho(\sigma^y \otimes \sigma^y)\rho^*(\sigma^y \otimes \sigma^y)]^{1/2}$, and corresponding entanglement of formation $\xi(C) = -\frac{1+\sqrt{1+C^2}}{2} \log_2 \frac{1+\sqrt{1+C^2}}{2} - \frac{1-\sqrt{1+C^2}}{2} \log_2 \frac{1-\sqrt{1+C^2}}{2}$, not only inconsistent with the entanglement entropy S , but also both exceed upper bound of physical entanglement for all γ and diverges at $\gamma \rightarrow J$ [see Fig. 5].

Now, we consider $\rho^{SVD} = \sqrt{\rho^\dagger \rho} / \text{Tr} \sqrt{\rho^\dagger \rho}$. For the state $|R_0\rangle$, we obtain

$$\rho^{SVD} = \frac{1}{2J} \begin{pmatrix} 0 & 0 & 0 & 0 \\ 0 & J+\gamma & -\sqrt{J^2 - \gamma^2} & 0 \\ 0 & -\sqrt{J^2 - \gamma^2} & J-\gamma & 0 \\ 0 & 0 & 0 & 0 \end{pmatrix}. \quad (A3)$$

The reduced density matrix for qubit 1 is now

$$\rho^{SVD,1} = \text{Tr}_2(\rho^{SVD}) = \frac{J+\gamma}{2J} |\uparrow\rangle\langle\uparrow| + \frac{J-\gamma}{2J} |\downarrow\rangle\langle\downarrow|, \quad (A4)$$

with entropy

$$S = -\frac{J+\gamma}{2J} \log_2 \frac{J+\gamma}{2J} - \frac{J-\gamma}{2J} \log_2 \frac{J-\gamma}{2J} \quad (A5)$$

now depends on γ and decreases monotonically to zero as $\gamma \rightarrow J$ (Fig. 5). The concurrence, obtained in this case $C = \sqrt{1 - (\gamma/J)^2}$ from the eigenvalues $\left\{ \frac{\sqrt{J^2 - \gamma^2}}{J}, 0, 0, 0 \right\}$ of $R = [\rho^{SVD}(\sigma^y \otimes \sigma^y)\rho^{SVD*}(\sigma^y \otimes \sigma^y)]^{1/2}$, and the corresponding entanglement of formation $\xi(C)$ is consistent with S (as per the requirement explained in⁷²). We have therefore considered ρ^{SVD} for concurrence computations whenever bi-orthogonal states are involved in the construction of density matrix. Note that, in systems satisfying usual orthogonality one has $\rho^{SVD} = \rho$.

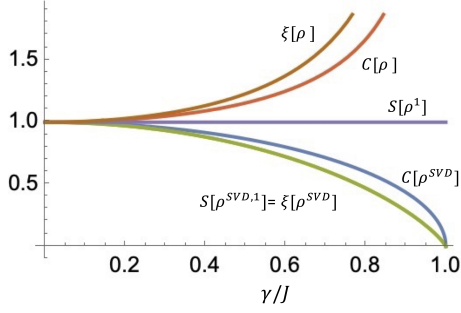


FIG. 5. Various entanglement measures, such as entropy (S), concurrence (C), and entanglement of formation (ξ), are presented for the bi-orthogonal pure state $|R_0\rangle\langle L_0|$. It is observed that the conventional density matrix ρ in Eq. (A2) yields inconsistent entanglement values, whereas measures derived from the SVD density matrix ρ^{SVD} in Eq. (A3) provide consistent results.

Appendix B: Analytical calculation of concurrence at low temperature limit $T \rightarrow 0$

Entanglement properties of the thermal state (given by Eq. (12)) is too cumbersome to obtain analytically. To gain analytical insights on the low temperature ($T \lesssim |E_1 - E_0|$) thermal entanglement, we approximate the thermal state consisting only ground and first excited state i.e

$$\rho = \frac{e^{-E_0/T}|R_0\rangle\langle L_0| + e^{-E_1/T}|R_1\rangle\langle L_1|}{e^{-E_0/T} + e^{-E_1/T}}, \quad (\text{B1})$$

which is in matrix form given by

$$\rho = \alpha \begin{pmatrix} e^{J\delta/T} & 0 & 0 & -e^{J\delta/T} \\ 0 & e^{\sqrt{J^2-\gamma^2}/T} & -\sqrt{\frac{J-\gamma}{J+\gamma}}e^{\sqrt{J^2-\gamma^2}/T} & 0 \\ 0 & -\sqrt{\frac{J+\gamma}{J-\gamma}}e^{\sqrt{J^2-\gamma^2}/T} & e^{\sqrt{J^2-\gamma^2}/T} & 0 \\ -e^{J\delta/T} & 0 & 0 & e^{J\delta/T} \end{pmatrix}, \quad (\text{B2})$$

where $\alpha = [2(e^{J\delta/T} + e^{\sqrt{J^2-\gamma^2}/T})]^{-1}$. In order to compute the concurrence, we obtain

$$\rho^{SVD} = \frac{\lambda}{2} \begin{pmatrix} e^{J\delta/T} & 0 & 0 & -e^{J\delta/T} \\ 0 & \sqrt{\frac{J+\gamma}{J-\gamma}}e^{\sqrt{J^2-\gamma^2}/T} & -e^{\sqrt{J^2-\gamma^2}/T} & 0 \\ 0 & -e^{\sqrt{J^2-\gamma^2}/T} & \sqrt{\frac{J-\gamma}{J+\gamma}}e^{\sqrt{J^2-\gamma^2}/T} & 0 \\ -e^{J\delta/T} & 0 & 0 & e^{J\delta/T} \end{pmatrix}, \quad (\text{B3})$$

and corresponding

$$R = \frac{\lambda}{2} \begin{pmatrix} e^{J\delta/T} & 0 & 0 & -e^{J\delta/T} \\ 0 & e^{\sqrt{J^2-\gamma^2}/T} & -\sqrt{\frac{J+\gamma}{J-\gamma}}e^{\sqrt{J^2-\gamma^2}/T} & 0 \\ 0 & -\sqrt{\frac{J-\gamma}{J+\gamma}}e^{\sqrt{J^2-\gamma^2}/T} & e^{\sqrt{J^2-\gamma^2}/T} & 0 \\ -e^{J\delta/T} & 0 & 0 & e^{J\delta/T} \end{pmatrix}, \quad (\text{B4})$$

where $\lambda = \sqrt{J^2 - \gamma^2} \left[(\sqrt{J^2 - \gamma^2} e^{J\delta/T} + J e^{\sqrt{J^2 - \gamma^2}/T}) \right]^{-1}$. Eigenvalues of R and corresponding concurrence reduces to the Eq. (16) and first of Eq. (17) in the main text. To derive the concurrence at $T = 0$, we note that C can also be written as

$$C = \begin{cases} \frac{\sqrt{J^2 - \gamma^2}}{J + \sqrt{J^2 - \gamma^2} e^{-(\sqrt{J^2 - \gamma^2} - J\delta)/T}} |e^{-(\sqrt{J^2 - \gamma^2} - J\delta)/T} - 1|, & \sqrt{J^2 - \gamma^2} - J\delta > 0 \\ \frac{\sqrt{J^2 - \gamma^2}}{J e^{-(J\delta - \sqrt{J^2 - \gamma^2})/T} + \sqrt{J^2 - \gamma^2}} |1 - e^{-(J\delta - \sqrt{J^2 - \gamma^2})/T}|, & J\delta - \sqrt{J^2 - \gamma^2} > 0 \end{cases} \quad (\text{B5})$$

Hence, the second of Eq. (17) in the main text readily follows.

Appendix C: General solution of H for arbitrary γ_1 and γ_2

For generic values of γ_1 and γ_2 , the asymmetric non-Hermitian Hamiltonian H reduces to

$$H = \begin{pmatrix} 0 & 0 & 0 & J\delta \\ 0 & 0 & J + \gamma_2 & 0 \\ 0 & J + \gamma_1 & 0 & 0 \\ J\delta & 0 & 0 & 0 \end{pmatrix}. \quad (\text{C1})$$

The right- and left-eigenvectors are given by

$$|R_{0,3}\rangle : \frac{1}{\sqrt{2}} \left(\sqrt{\frac{J+\gamma_2}{J+\gamma_1}} |\uparrow\downarrow\rangle \mp |\downarrow\uparrow\rangle \right), \quad |R_{1,2}\rangle : \frac{1}{\sqrt{2}} (|\uparrow\uparrow\rangle \mp |\downarrow\downarrow\rangle) \\ |L_{0,3}\rangle : \frac{1}{\sqrt{2}} \left(\sqrt{\frac{J+\gamma_1}{J+\gamma_2}} |\uparrow\uparrow\rangle \mp |\downarrow\downarrow\rangle \right), \quad |L_{1,2}\rangle = |R_{1,2}\rangle, \quad (\text{C2})$$

with corresponding energies

$$E_{0,1,2,3} = \left\{ -\sqrt{(J + \gamma_1)(J + \gamma_2)}, -J\delta, J\delta, \sqrt{(J + \gamma_1)(J + \gamma_2)} \right\}.$$

The ground state of the system is determined by the minimum value between E_0 and E_1 , which depends on the parameters $\gamma_{1,2}$ and δ . When $E_0 < E_1$, specifically when $(J + \gamma_1)(J + \gamma_2) > J^2\delta^2$, the ground state corresponds to the non-maximally entangled state $|R_0\rangle$. Conversely, if $E_1 < E_0$, meaning $(J + \gamma_1)(J + \gamma_2) < J^2\delta^2$, the ground state is the Bell state $|R_1\rangle$. The concurrence for the Bell state satisfies $C(|R_1\rangle\langle L_1|) = 1$, whereas the concurrence for the non-maximally entangled state $|R_0\rangle$ is given by Eq. (19) in the main text which is always less than one. As a result, both the nature of the ground state and its entanglement properties at zero temperature ($T = 0$) undergo changes at parameter values where $E_0 = E_1$, specifically when $(J + \gamma_1)(J + \gamma_2) = J^2\delta^2$ is satisfied.

Acknowledgments

The research was supported by the ANRF Grant (MTR/2023/000249) and a Seed Grant from IISER Berhampur, India.

- ¹Y. Ashida, Z. Gong and M. Ueda, *Adv. Phys.* **69**, 249-435 (2021).
- ²I. Rotter, *J. Phys. A: Math. Theor.* **42**, 153001 (2009).
- ³W. D. Heiss, *J. Phys. A: Math. Theor.* **45**, 444016 (2012).
- ⁴S. K. Özdemir, S. Rotter, F. Nori and L. Yang, *Nature Materials* **18**, 783–798 (2019).
- ⁵R. El-Ganainy, K. G. Makris, M. Khajavikhan, Z. H. Musslimani, S. Rotter and D. N. Christodoulides, *Nature Phys.* **14**, 11–19 (2018).
- ⁶L. Feng, R. El-Ganainy and L. Ge, *Nature Photon.* **11**, 752–762 (2017).
- ⁷K. Kawabata, Y. Ashida, M. Ueda, *Phys. Rev. Lett.* **119**, 190401 (2017).
- ⁸L. Xiao, K. Wang, X. Zhan, Z. Bian, K. Kawabata, M. Ueda, W. Yi, and P. Xue, *Phys. Rev. Lett.* **123**, 230401 (2019).
- ⁹B. Dora, M. Heyl, R. Moessner, *Nat. Commun.* **10**, 2254 (2019).
- ¹⁰Y.-L. Zhou, X.-D. Yu, C.-W. Wu, X.-Q. Li, J. Zhang, W. Li, and P.-X. Chen, *Phys. Rev. Research* **5**, 043036 (2023).
- ¹¹K. Sun and W. Yi, *AAPPS Bulletin* **34**, 22 (2024).
- ¹²Y. Wu, W. Liu, J. Geng, X. Song, X. Ye, C.-K. Duan, X. Rong, and J. Du, *Science* **364**, 878-880 (2019).
- ¹³J.-W. Zhang et al., *Nat. Commun.* **13**, 6225 (2022).
- ¹⁴Y. Wu, Y. Wang, X. Ye, W. Liu, Z. Niu, C.-K. Duan, Y. Wang, X. Rong and J. Du, *Nat. Nanotechnol.* **19**, 160–165 (2024).
- ¹⁵J. Wen, G. Qin, C. Zheng, S. Wei, X. Kong, T. Xin, G. Long, *npj Quantum Information* **6**, 28 (2020).
- ¹⁶L. Ding, K. Shi, Q. Zhang et al., *Phys. Rev. Lett.* **126**, 083604 (2021).
- ¹⁷L. Ding et al., *Phys. Rev. A* **105**, L010204 (2022).
- ¹⁸M.-M. Cao, K. Li, W.-D. Zhao et al., *Phys. Rev. Lett.* **130**, 163001 (2023).
- ¹⁹E. Zhao et al., *Nature* **637**, 565-573 (2025).
- ²⁰Z. Ren et al., *Nature Physics* **18**, 385-389 (2022).
- ²¹J. Li, A. K. Harter, J. Liu, L. de Melo, Y. N. Joglekar, and L. Luo, *Nat. Comm.* **10**, 855 (2019).
- ²²W. Chen, M. Abbasi, Y. N. Joglekar, and K. W. Murch, *Phys. Rev. Lett.* **127**, 140504 (2021).
- ²³M. Naghiloo, M. Abbasi, Y. N. Joglekar & K. W. Murch, *Nature Physics* **15**, 1232–1236 (2019).
- ²⁴H. Gao, K. Sun, D. Qu, K. Wang, L. Xiao, W. Yi, and P. Xue, *Phys. Rev. Lett.* **134**, 146602 (2025).
- ²⁵L. Xiao et al., *PRX Quantum* **2**, 020313 (2021).
- ²⁶P. M. Harrington, E. J. Mueller, K. W. Murch, *Nat. Rev. Phys.* **4**, 660-671 (2022).
- ²⁷M. A. Selim et al., *Science* **387** 1424-1428 (2025).
- ²⁸Z-Z Li, W. Chen, M. Abbasi, K. W. Murch and K. B. Whaley, *Phys. Rev. Lett.* **131**, 100202 (2023)
- ²⁹S. Khandelwal, W. Chen, K. M. Murch, and G. Haack, *Phys. Rev. Lett.* **133**, 070403 (2024).
- ³⁰P.-R. Han, F. Wu, X.-J. Huang et al., *Phys. Rev. Lett.* **131**, 260201 (2023).
- ³¹J. Zou, S. Zhang, and Y. Tserkovnyak, *Phys. Rev. B* **106**, L180406 (2022).
- ³²C. G. Feyisa, J-S You, H-Y Ku and H H Jen, *Quantum Sci. Technol.* **10**, 025021 (2025)
- ³³S. Longhi, *Opt. Lett.* **50**, 5101-5104 (2025).
- ³⁴Y.-B Qian, L Tang, D-G Lai, and B-P Hou, *Phys. Rev. A* **112**, 043548 (2025)
- ³⁵A. Kumar, K. W. Murch, and Y. N. Joglekar, *Phys. Rev. A* **105**, 012422 (2022).
- ³⁶Y.-X Zhang, Z.-T. Zhang, X.-Z Wei, B.-L Liang, F. Mei, and Z.-S Yang, *J. Phys. B* **57**, 085501 (2024)
- ³⁷P. Chang, J. You, X. Wen and S. Ryu, *Phys. Rev. Research* **2**, 033069 (2020).
- ³⁸L. S. Lima, *Physica E* **174**, 116356 (2025).
- ³⁹L. S. Lima, *Physica E* **156**, 115861 (2024).
- ⁴⁰F. Rottoli, M. Fossati and P. Calabrese, *J. Stat. Mech.* 063102 (2024).
- ⁴¹C.-Y. Ju, A. Miranowicz, G.-Y. Chen, and F. Nori, *Phys. Rev. A* **100**, 062118 (2019)
- ⁴²C.-Y. Liu, C. G. Feyisa, M. S. Hasan, and H H Jen, *J. Phys. B* **58**, 075501 (2025).
- ⁴³T. E. Lee, F. Reiter, and N. Moiseyev, *Phys. Rev. Lett.* **113**, 250401 (2014).
- ⁴⁴P. Kumar, K. Snizhko, Y. Gefen, and B. Rosenow, *Phys. Rev. A* **105**, L010203 (2022).
- ⁴⁵V. L. Duc, M. Nowotarski, and J. K. Kalaga, *Symmetry* **13**, 203 (2021).
- ⁴⁶Y. L. Gal, X. Turkeshi and M. Schiró, *SciPost Phys.* **14**, 138 (2023).
- ⁴⁷D. F. Muñoz-Arboleda, R. Arouca, and C. Morais Smith, *Phys. Rev. B* **110**, 115135 (2024).
- ⁴⁸Y.L. Fang et al., *Phys. Rev. Research* **4**, 033022 (2022).
- ⁴⁹X. Turkeshi, and M. Schiró, *Phys. Rev. B* **107**, L020403 (2023).
- ⁵⁰C.-Z. Lu, X. Deng, S.-P. Kou, and G. Sun, *Phys. Rev. B* **110**, 014441 (2024).
- ⁵¹K. Kawabata, T. Numasawa, and S. Ryu, *Phys. Rev. X* **13**, 021007 (2023).
- ⁵²S.-Z. Li, X.-J. Yu, and Z. Li, *Phys. Rev. B* **109**, 024306 (2024); L. Zhou, *Phys. Rev. B* **109**, 024204 (2024).
- ⁵³S.-L. Chen, G.-Y. Chen, and Y.-N. Chen, *Phys. Rev. A* **90**, 054301 (2014).
- ⁵⁴M.C. Arnesen, S. Bose, V. Vedral, *Phys. Rev. Lett.* **87**, 017901 (2001).
- ⁵⁵G. L. Kamta, and A. F. Starace, *Phys. Rev. Lett.* **88**, 107901 (2002).
- ⁵⁶L. Amico, R. Fazio, A. Osterloh, and V. Vedral, *Rev. Mod. Phys.* **80**, 517 (2008).
- ⁵⁷D. Gunlycke, V. M. Kendon, and V. Vedral, *Phys. Rev. A* **64**, 042302 (2001).
- ⁵⁸X. Wang, *Phys. Rev. A* **64**, 012313 (2001).
- ⁵⁹F. Reiter and Anders S. Sørensen, *Phys. Rev. A* **85**, 032111 (2012).
- ⁶⁰F. Minganti, A. Miranowicz, R. W. Chhajlany, and F. Nori, *Physical Review A* **100**, 062131 (2019).
- ⁶¹F. Minganti, A. Miranowicz, R. W. Chhajlany, I. I. Arkhipov and F. Nori, *Phys. Rev. A* **101**, 062112 (2020).
- ⁶²C. Gardiner and P. Zoller, *Quantum Noise* (Springer, Berlin, 2004).
- ⁶³A. Metelmann and A. A. Clerk, *Physical Review X* **5**, 021025 (2015).
- ⁶⁴F. Song, S. Yao, and Z. Wang, *Phys. Rev. Lett.* **123**, 170401 (2019).
- ⁶⁵S. Takemori, K. Yamamoto, and A. Koga, *Phys. Rev. Lett.* **135**, 266002 (2025).
- ⁶⁶H. Pichler, T. Ramos, A. J. Daley, and P. Zoller, *Phys. Rev. A* **91**, 042116 (2015).
- ⁶⁷K. Stannigel, P. Rabl and P. Zoller, *New J. Phys.* **14** 063014 (2012).
- ⁶⁸D. C. Brody, *J. Phys. A* **47**, 035305 (2013).
- ⁶⁹Y. Li, P. P. Zhang, L. Z. Hu, Y. L. Xu and X. M. Kong, *Quantum Inf. Process.* **22**, 277 (2023).
- ⁷⁰Z. Yunpeng, Y. Shun, C. Guohao, H. Halimjan and A. Abliz, *Int. J. Theor. Phys.* **64**, 90 (2025).
- ⁷¹A. J. Parzygnat, T. Takayanagi, Y. Takic and Z. Weic, *JHEP* **12**, 123 (2023).
- ⁷²W.K. Wootters, *Phys. Rev. Lett.* **80**, 2245 (1998).
- ⁷³D. A. Abanin, E. Altman, I. Bloch, and M. Serbyn, *Rev. Mod. Phys.* **91**, 021001 (2019).